Journal of Sailing Technology 20XX, volume X, issue X, pp. XX – XX.
The Society of Naval Architects and Marine Engineers.

Dynamic Performance Prediction for Wind-Powered Ships

Martin Kjellberg
RISE Research Institutes of Sweden AB, Sweden, martin.kjellberg@ri.se.

Adam Persson
RISE Research Institutes of Sweden AB and Chalmers University of Technology, Sweden.

Frederik C. Gerhardt
RISE Research Institutes of Sweden AB, Sweden.

Sofia Werner
RISE Research Institutes of Sweden AB, Sweden.

Manuscript received [Month] [day], [year]; revision received [Month] [day], [year]; accepted [Month] [day], [year].

Abstract. The need to reduce green-house gas emissions has renewed the interest in wind propulsion for commercial cargo vessels. When designing such modern "sailing" ships, naval architects often lean on methods and tools originally developed for the design of sailing yachts. The most common tool today is the steady-state Performance Prediction Program (PPP), typically used to predict quantities like speed, leeway, heel of the vessel when sailing in a range of wind directions and wind speeds. Steady state PPPs are very efficient and can be used to rapidly assess a large number of design alternatives. PPPs are, however, not able to consider dynamic effects such as unsteady sail forces due to ship motions in waves or the turbulent structure of the natural wind. In this paper we present time-domain simulations with a Dynamic Performance Prediction Program (DPPP) that can take the "unsteadiness" of the natural environment into account. The program is based on coupling an unsteady 3D fully nonlinear potential flow hydrodynamic solver to an efficient lifting-line aerodynamic model. Particular attention is paid to a recently implemented unsteady aerodynamic model that employs an indicial response method based on Wagner's function. The usefulness of such advanced simulations for performance prediction in moderate environmental conditions is investigated for a wind-powered cargo vessel with wing sails. Control system strategies such as sheeting of the wing sails close to stall are studied.

Keywords: wind propulsion; wing sails; DPPP; Indicial Response Method.

NOMENCLATURE

C_l	Aerodynamic lift coefficient (2D) [-]
$C_{l\infty}$	Aerodynamic lift coefficient (2D, steady-state) [-]
D	Propeller diameter [m]
H_s	Significant wave height [m]
K_{xx}, K_{yy}, K_{zz}	Roll, pitch, and yaw radius of gyration, respectively [m]
RT	Turbulent viscosity ratio [-]
T_z	Zero-up crossing period [s]
T_p	Oscillation period
V	Wind velocity [m s^{-1}]
p	Pressure [Pa]
s	Nondimensional time [-]
s_{rudder}	Rudder span [m]

t	Time [s]
u_{10}	Mean wind speed at a height 10 m [m s^{-1}]
c	Chord length [m]
c_{r}, c_{t}	Rudder root and tip chord length, respectively [m]
Ω	Rudder sweep angle [°]
α	Angle of attack [-]
α_e	Effective angle of attack [-]
∇	Displacement [m^3]
ϕ	Indicial response function [-]
ρ	Fluid density [kg m^{-3}]
σ	Dummy variable for nondimensional time [-]
τ	Dummy variable for time [s]
CFD	Computational Fluid Dynamics
DPPP	Dynamic Performance Prediction Program
GM	Metacentric height
IRM	Indicial Response Method
KG	Vertical center of gravity
URANS	Unsteady Reynolds-Averaged Navier-Stokes

1. INTRODUCTION

Wind propulsion is emerging as an effective method to enhance the efficiency of transportation and lower the emissions of commercial cargo ships. The design framework for conventionally powered vessels is well-defined and supported by mature tools. However, the scenario alters significantly for the design of wind-propelled ships. The development of primary wind-powered vessels introduces numerous novel challenges, particularly regarding performance prediction, necessitating fresh demands on design tools. Before this background, the maritime industry is actively involved in creating new simulation and analysis tools.

The design of primary wind-propelled vessels predominantly relies on steady-state PPP simulations and time-domain simulations are relatively rare. The steady-state approach has its limitations in terms of the phenomena that can be analyzed. While some effects, like added resistance due to waves, can be adequately assessed using this method, it falls short in modeling more transient phenomena. Examples of such phenomena include the helm action in response to induced motions in a seaway, particularly under transient wind gusts or large-scale turbulence in the wind. The variability in ship motions and the wind field also impacts the relative inflow to the wind propulsion units. Time-domain methods are essential to model and understand these effects. However, due to the significant increase in computational effort required, time-domain simulations are more apt for studying short-term performance aspects. These aspects include ship maneuvering, course-keeping in waves, sheeting strategies, and the development of rig-control algorithms.

While the transient aerodynamic response has not yet been considered in time-domain simulations of sailing vessels, the topic has been explored by several authors working within the field of yacht sail aerodynamics (Roux et. al., 2008); (Gerhardt et al., 2011); (Fossati and Muggiasca, 2010); (Augier et. al., 2012 & 2013). Several methods, both experimental and numerical, have been used to characterize the transient aerodynamic response, and describe how it deviates from the static or quasi-static response. The conclusions are clear; there can be significant transient effects on yacht sails, causing a reduction in lift amplitude, a shift in phase, and hysteresis, as is described by Augier et. al. (2012, 2013). Gerhardt et. al. (2011) concluded that for performance prediction on time-scales shorter than the wave period, a model capable of considering the transient aerodynamic response should be used. However, the impact of the transient aerodynamic response on the dynamics of a sailing vessel is not known.

This paper examines the impact of employing unsteady versus quasi-static modeling of circulatory lift on the performance predictions of a fully sailing car carrier. We introduce an indicial response method (IRM) for modeling unsteady circulatory lift force, integrating it into an existing time-domain approach implemented in the commercial panel code SHIPFLOW MOTIONS. This approach is based on an unsteady 3D fully nonlinear potential flow hydrodynamic model, enhanced by the inclusion of viscous maneuvering derivatives and an efficient lifting-line aerodynamic method. Additionally, the model includes a representation of a short-crested irregular incident wave field and a simple spatio-temporal model for atmospheric turbulence (Kjellberg et al., 2023).

2. UNSTEADY CIRCULATORY LIFT

The modelling of unsteady circulatory lift force is based on the indicial response method (IRM), within the framework of thin airfoil theory. The IRM, specifically the Wagner function, (Wagner,1925), which describes the transient lift response of an airfoil to a step change in the angle of attack before reaching a new steady state, is well suited for analyzing the transient lift response of an airfoil. A key component of this method is the convolution of the Wagner function with the time history of angle of attack changes. This convolution process effectively captures the ‘memory’ of the airfoil, reflecting how past states influence current aerodynamic conditions.

We employ the Duhamel integral to generalize the Wagner function for arbitrary, time-varying angles of attack. This approach allows for a comprehensive representation of the airfoil's lift response over time, considering the cumulative effect of previously shed vortices in the wake.

2.1 Indicial Response Method

The Indicial Response Method is used to describe the response of a system to a sudden change, or "indicial" input, such as a step change in the angle of attack. The response function, known as the indicial response, characterizes how the system behaves over time following this sudden change.

Wagner (1925), using thin airfoil theory, derived the so-called Wagner function which specifically describes the indicial response of a thin airfoil as a function of the nondimensional time. The nondimensional is defined as:

$$s(t) = \frac{2}{c}\int_0^t V(t)\,dt\,, \tag{1}$$

where $V(t)$ is the time-varying fluid velocity, t is time and c is the chord length. This non-dimensional timescale represents the distance travelled by the wake in the free stream, although we approximate it by using the mean wind speed. The Wagner function $\phi(s)$, normalized by 2π, can be approximated as (Jones, 1938):

$$\phi(s) = 1 - 0.165e^{-0.0455s} - 0.335e^{-0.3s}. \tag{2}$$

This normalized Wagner function, plotted in Figure 1, can be seen as an indicial response function and represents the influence of shed vortices on the instantaneous angle of attack of an airfoil.

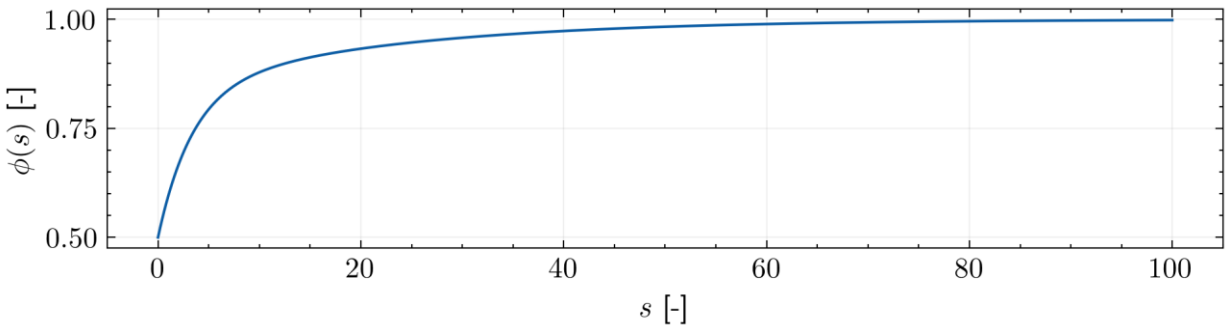

Figure 1. Plot of the indicial response function as function of nondimensional time, $\phi(s)$ (Jones' approximation of the Wagner function, normalized by 2π).

2.2 Generalization to Time-Varying Angle of Attack

In the context of sailing dynamics, the angle of attack varies continuously and not just a series of step changes. The Duhamel integral (Kármán and Biot, 1940) can be used to generalize the indicial response to arbitrary, time-varying angle of attack by convolving the indicial response function $\phi(s)$ with the time history of the angle of attack changes. Using the Duhamel integral, the lift coefficient at time t is given by:

$$C_l(t) = \frac{\partial C_{l\infty}\big(\alpha(t=0)\big)}{\partial\alpha}\alpha(t=0)\phi\big(s(t=0)\big) + \int_0^t \phi\big(s(t)-s(\tau)\big)\frac{\partial C_{l\infty}\big(\alpha(t)\big)}{\partial\alpha}\frac{d\alpha}{d\tau}d\tau \tag{3}$$

The first term represents the effect of the induced downwash from the starting vortex generated at time $t = 0$. The second term is an integral that accounts for the accumulated effect of the angle of attack history and corresponding shed vorticity. It integrates the product of the rate of change of angle of attack $d\alpha/d\tau$ and the indicial response function $\phi(s)$ evaluated at $s(t) - s(\tau)$, thereby accounting for the influence of past changes in angle of attack on the current lift.

We can subsequently express the time-varying lift coefficient as:

$$C_l(t) = \frac{\partial C_{l\infty}(\alpha(t))}{\partial \alpha}\left[\alpha(t=0)\phi\big(s(t=0)\big) + \int_0^t \phi\big(s(t) - s(\tau)\big)\frac{d\alpha}{d\tau}d\tau\right] = \frac{\partial C_{l\infty}(\alpha(t))}{\partial \alpha}\alpha_e(t) \quad (4)$$

The terms within the bracket can be seen as an effective angle of attack $\alpha_e(t)$ incorporating the effects of the previously shed vortices in the unsteady wake.

For a discrete system where the angle of attack is sampled at non-dimensional times $s = s_0, \sigma_1, \dots, \sigma_i, s$ separated by a constant time step Δs, we can write the effective angle of attack α_e in a discrete form. This involves approximating the continuous integral with a summation over the discrete time steps. Given that $\alpha_e(t)$ is defined as:

$$\alpha_e(t) = \alpha(t=0)\phi\big(s(t=0)\big) + \int_0^t \phi\big(s(t) - s(\tau)\big)\frac{d\alpha}{d\tau}d\tau\,, \quad (5)$$

the discrete system becomes:

$$\alpha_e(s) = \alpha(s_0)\phi(s) + \sum_{i=1}^{\mathrm{n}} \phi(s - \sigma_i)\frac{d\alpha}{ds}(\sigma_i)\Delta s \quad (6)$$

Here, $\frac{d\alpha}{ds}(\sigma_i)\Delta s$ represents the change in the angle of attack between adjacent time steps, which can be approximated as $\Delta\alpha_i \approx \alpha(\sigma_i) - \alpha(\sigma_{i-1})$ and we get:

$$\alpha_e(s) = \alpha(s_0)\phi(s) + \sum_{i=1}^{\mathrm{n}} \phi(s - \sigma_i)\Delta\alpha_i \quad (7)$$

The first term represents the downwash induced by the starting vortex generated at time $t = 0$ and it will have a waning influence on the total lift as time evolve and the distance to the starting vortex grows large.

In vectorized form the resulting equation for $\alpha_e(s)$ can be written as a dot product:

$$\alpha_e(s) = \phi(s - \boldsymbol{\sigma}) \cdot \boldsymbol{\Delta\alpha} \quad (8)$$

where $\boldsymbol{\sigma} = [s - \sigma_0, s - \sigma_1, \dots, s - \sigma_n]$ is a time-shift vector. This vector represents the discrete time steps in the past relative to the current nondimensional time s, with each element $s - \sigma_i$ indicating the time delay since the angle of attack was sampled at time σ_i. The vector $\boldsymbol{\Delta\alpha}$ contains the history of discrete changes in angle of attack between subsequent time-steps, corresponding to the same time intervals as in $\boldsymbol{\sigma}$.

2.3. Validation With Numerical Data

In order to confirm that the model works as intended, 2D URANS CFD simulations were performed for the section of the wing sails used on the Wind-Powered Car Carrier, a symmetrical NACA0015

section. Time-histories of lift and drag were obtained as the section was subjected to a forced oscillation perpendicular to the wind direction, resulting in a variation of angle of attack. The case parameters were selected to approximately represent those expected in the subsequent DVPP simulations (see Sections 3 and 4), with a wind speed of 15 m s^{-1}, a mean angle of attack of 16°, an angle of attack amplitude of 4°, and a motion period of 8 s. The predictions from the IRM based model was then compared to the time-histories predicted by URANS CFD, allowing the validity of the model to be evaluated, see Section 2.3.2.

2.3.1 CFD Setup

The 2D simulations were performed in Siemens Simcenter STAR-CCM+ 2210-R8, using the segregated incompressible, implicit unsteady, solver with a SIMPLE pressure-velocity coupling scheme. A second-order convective scheme and a second-order temporal scheme is used. The simulations were initialised by simulating 60 seconds without grid motion, using a time step of Δt = 0.05 s. The grid motion was then ramped using a fifth-order polynomial function, ensuring a smooth change in grid velocity and acceleration, while the jerk signal is continuous. During the unsteady phase, a time step of $\Delta t = T_p/200$ was used, where T_p is the oscillation period. A total of ten oscillation periods were simulated. In each time step, inner iterations were performed until the normalised residuals had been reduced by three orders of magnitude. Turbulence was modelled using the one-equation Spalart-Allmaras model. A low y+ wall treatment was used, meaning that the boundary layer is resolved into the viscous sublayer.

A rectangular computational domain was used, extending 50c upstream, above and below the section, and 100c downstream of the section. On the upstream and top/bottom boundaries, a velocity inlet condition was used, with velocity V = 15 m s^{-1}. A pressure outlet condition is used on the downstream boundary with pressure p = 0.0 Pa. On the inlet and outlet boundaries, ambient turbulence is specified by turbulent viscosity ratio RT = 3, as suggested by Spalart and Rumsey (2007). A no-slip smooth wall condition is used on the wall surfaces. An unstructured hexahedral grid with 95 000 cells was generated, with a cell size on the wing corresponding to 256 cells per chord length. An additional refinement was used on the leading and trailing edges, dividing overall wing cell size by a factor of three. 40 prism layers were generated to resolve the gradients in the boundary layer, and the first cell spacing was adapted to ensure that the maximum y+ value remained below 0.5.

The simulation setup and grid configuration are very similar to that presented in Persson et al. (2023), where the discretisation uncertainty for lift coefficient has been shown to be very low (<1%) and the temporal discretisation has been shown to be sufficient.

2.3.2 Validation Results

Comparing the IRM against the numerical results in Figure 2 shows a very good agreement, both in terms of amplitude and phase. At a time of 60 s, the lift coefficient has reached the same level as the steady state value. The initial response due to the transient start is also well captured.

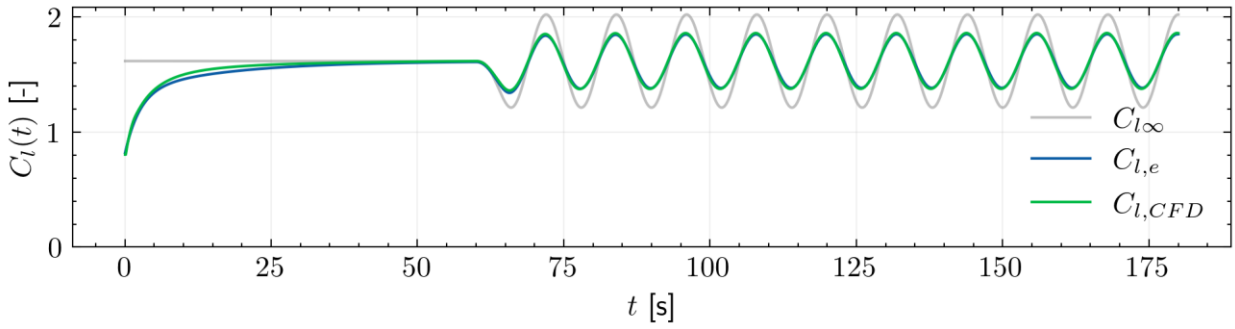

Figure 2 Comparison of quasi-static, IRM-based, and numerical lift coefficient for a NACA0015 with a wind speed of 15 m s^{-1}, a mean angle of attack of 16°, an angle of attack amplitude of 4°, and a motion period of 8 s.

3. CASE DESCRIPTION

The test case studied here is an early version of the Oceanbird concept. This concept for a wind-powered car carrier was developed as a research test case around 2021 by a Swedish consortium, consisting of Wallenius Marine, KTH Royal Institute of Technology and SSPA Sweden AB. The ship is 206 m long, displaces around 30 000 ton and should be able to transport 7 000 car units across the Atlantic Ocean in 12 days, which corresponds to an average speed of 10 knots. Four 80 m tall (from deck) rigid wing sails will drive the ship, only occasionally supported by conventional propulsion, reducing the emissions by about 90 percent. The main particulars of the vessel are summarized in Table 1 and the vessel with the wing sails are shown in Figure 3. The ship has twin propellers and twin spade rudders.

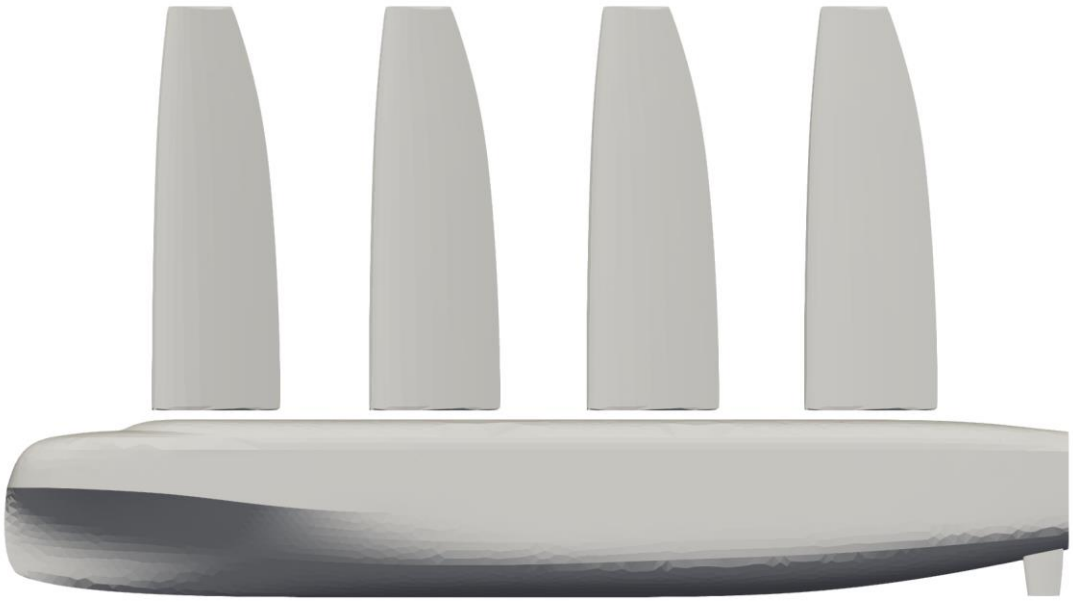

Figure 3 Side view of the Wind-Powered Car Carrier

The rudders of the vessel are controlled by an autopilot (PID) set for heading control and configured with the following PID parameters: $K_P = 2, T_I = 100$ s and $T_D = 2$ s. The sails are sheeted for a target mean local geometric angle of attack α over the span in both the quasi-static and the unsteady indicial response method. In this work, the target angle of attack is set to 16°, slightly below the angle of attack of maximum lift at 19°.

Table 1 Main particulars of the Wind-Powered Car Carrier

Parameter	Symbol	Value	Unit
Length between perpendiculars	L_{PP}	206.60	m
Beam	B	39.00	m
Draft	T	8.50	m
Air draft	T_{air}	105.00	m
Sail span	s_{sail}	80.00	m
Max sail chord	$c_{\text{max, sail}}$	26.50	m
Total sail area	$A_{\text{tot, sail}}$	7360.00	m^2
Sail section profile	-	NACA0015	m
Displacement	∇	30843.00	m^3
Metacentric height	GM	5.60	m
Vertical center of gravity	KG	18.00	m
Roll gyradius	I_{xx}	13.65	m
Pitch and yaw gyradii	I_{yy}, I_{zz}	51.65	m
Rudder span	s_{rudder}	7.18	m
Rudder root chord	c_{r}	7.93	m
Rudder tip chord	c_{t}	6.30	m
Rudder sweep angle	Ω	0.00	°
Propeller diameter	D	5.00	m

3.1 Sailing Test Conditions

The vessel is fully sailing in moderate environmental conditions of short-crested waves based on a JONSWAP spectrum and sea state 4 ($H_s = 1.88$ m), with a corresponding true wind speed of 10 m s^{-1}. The spatial variation of the wind field resulting from the spatio-temporal wind model can be seen in Figure 4 as it affects the local wind velocity along the ¾-chord line of each wing.

A simple sheeting strategy based on continuous sheeting for a target averaged local angle of attack of 16° is employed but with two different sheeting rates: a fast rate of 3.0° s^{-1} and a slow rate of 0.125° s^{-1}. The fast rate is fast enough for the wings to react reasonably well to the varying inflow and the slow rate is still fast enough for the wings to be trimmed for lower frequency gusts and lulls. The test matrix is presented in Table 2.

Table 2 Test matrix.

Case notation	Lift model	Sheeting rate [° s^{-1}]	H_s [m]	T_z [s]	u_{10} [m s^{-1}]	TWA [°]
SS4-50-QS-F	Quasi-static	3.000	1.88	6.2	10.0	50
SS4-50-QS-S	Quasi-static	0.125	1.88	6.2	10.0	50
SS4-50-IRM-F	IRM	3.000	1.88	6.2	10.0	50
SS4-50-IRM-S	IRM	0.125	1.88	6.2	10.0	50

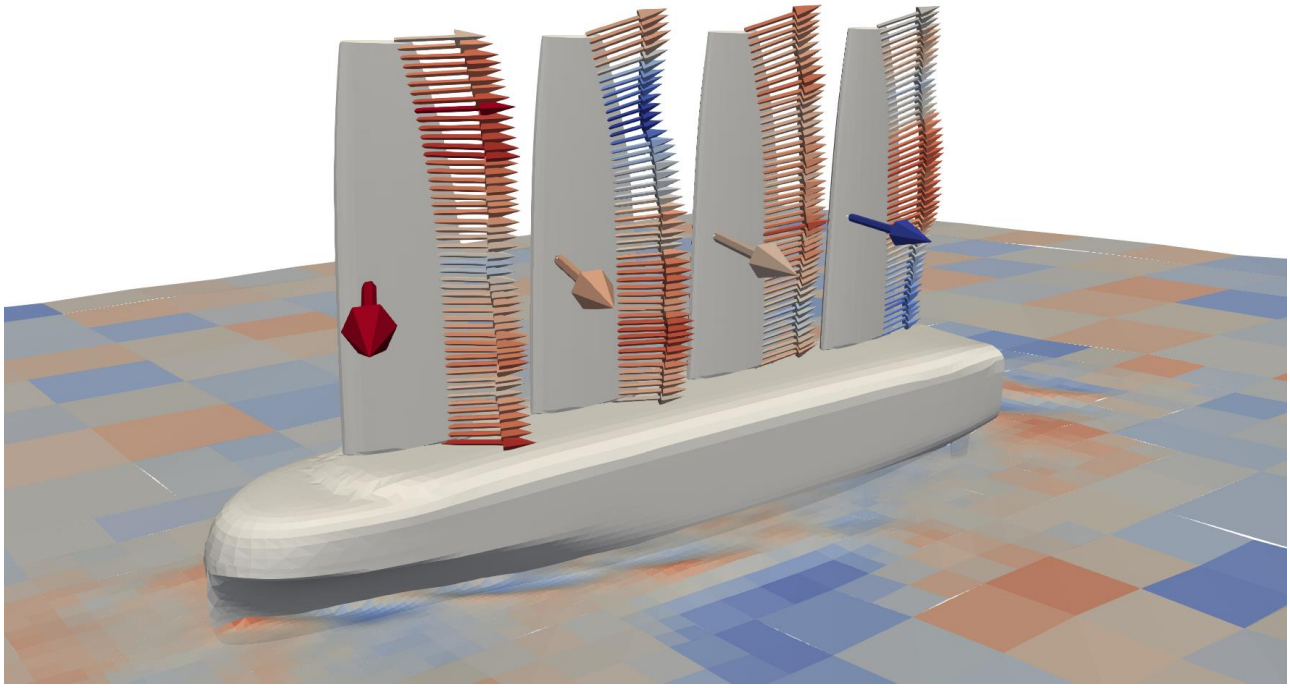

Figure 4 Snapshot of the Wind-Powered Car Carrier sailing in SS4, TWA=50° and TWS=10 m s^{-1}**.** The arrows along the ¾-chord line represent the local apparent wind velocity used as boundary condition values for the lifting line model. The arrows perpendicular to the wing represent the total aerodynamic force acting on each wing sail.

4. COMPARISON OF SAILING PERFORMANCE

Comparing the time series of the simulations with quasi-static modelling of the circulatory lift to those based on the IRM, it becomes clear that the effect is small for this case. Figure 5 shows the averaged local angle of attack (effective angle of attack in the case of the IRM) over the span of each wing, with wing 1 being the foremost and the wing 4 being the aftmost wing. Initially, the transient high lift generated by the wings at the beginning of the simulations are clearly dampened and reduced by a factor of two after which the continued time record of the lift for the IRM shows a more dampened response, which is exactly what is expected. However, the difference is not large and is only displayed on the higher frequencies related to the turbulent wind and not the lower frequencies related to larger scale turbulence.

Continuing with Figure 6, showing the time series of the boom angles, the difference between the two models is minimal for this case. It should be noted that the sheet controller is comparing the target angle of attack against the geometrical angle of attack and not the effective angle of attack in the IRM method. This is just a choice that was made and letting the controller consider the effective angle of attack might have improved the efficiency somewhat, although most likely to a marginal extent.

Finally, in Figure 7, some of the global performance variables are plotted against time: Speed over ground (SOG), heel angle, leeway angle, and rudder angle. Here, the difference between the results from either method are very similar, indicating that the effect of modelling these unsteady effects have a negligible effect on the overall performance prediction in moderate environmental conditions like these. If anything, the quasi-static method shows a somewhat more dampened roll motion amplitude, which is the expected behavior, although it should be remembered that the roll motions are indeed very small in these conditions to begin with.

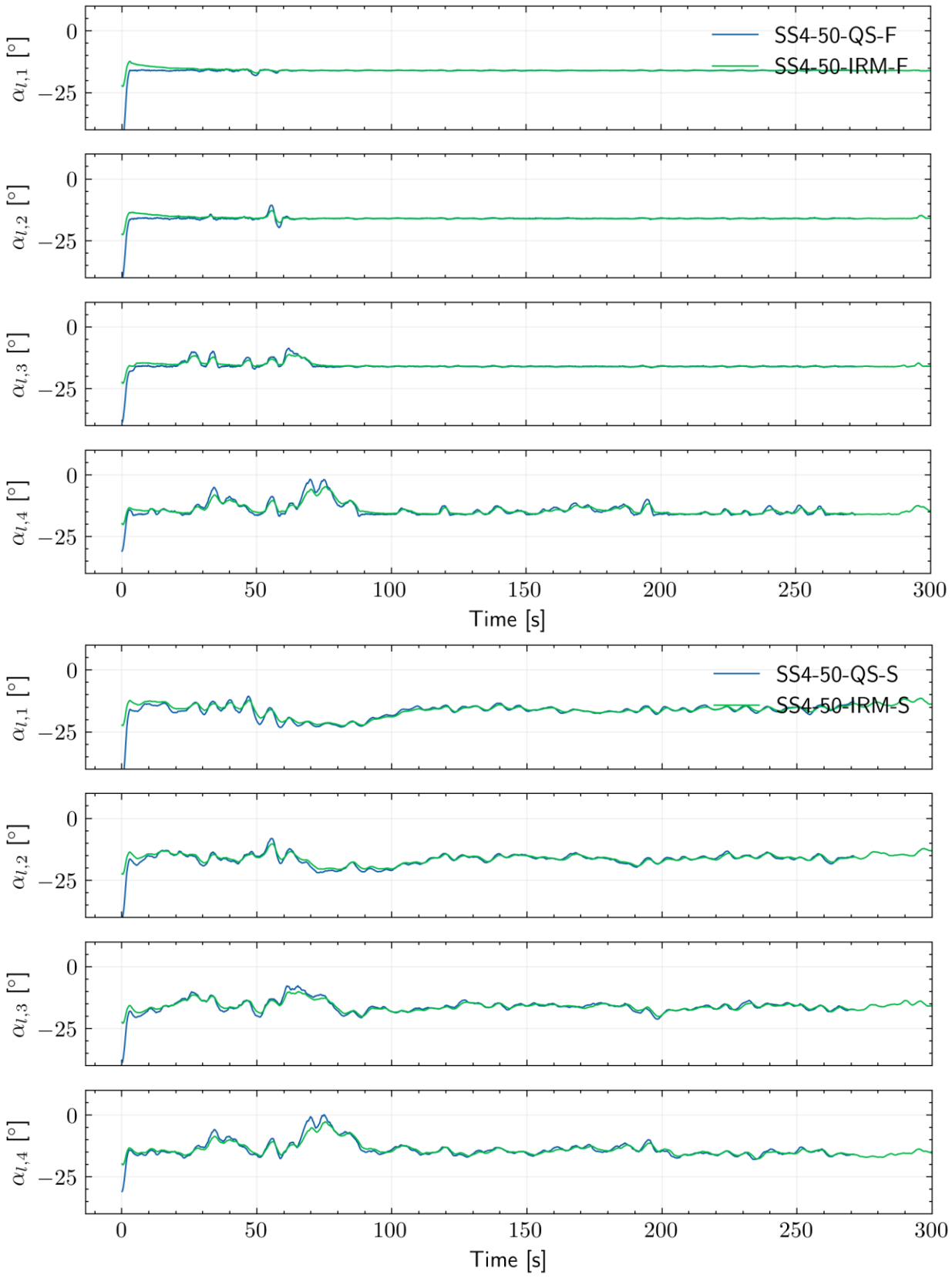

Figure 5 Time series of average local effective angle of attack over the wings (Top: Fast sheeting rate; Bottom: Slow sheeting rate).

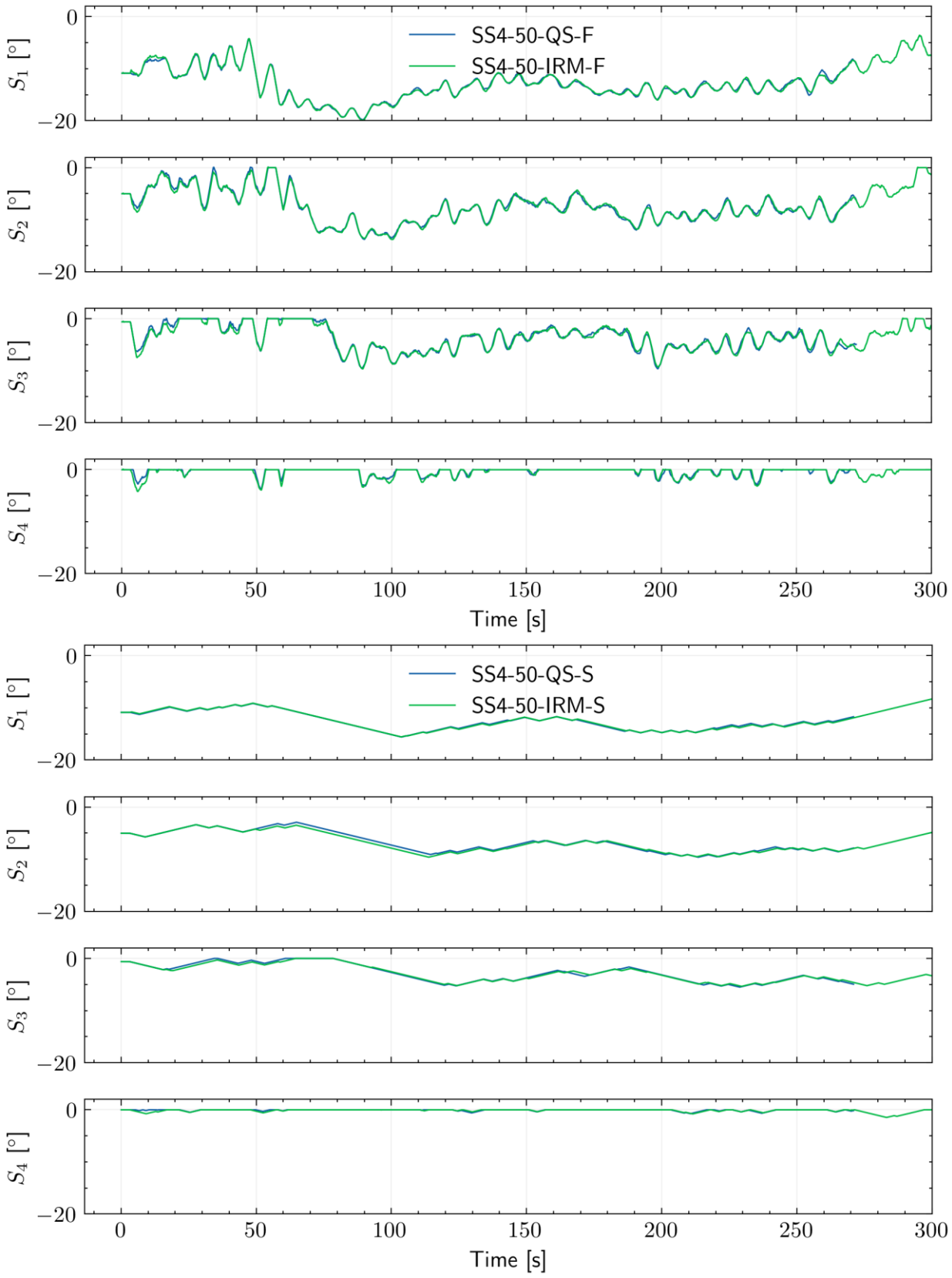

Figure 6 Time series of sheet/boom angles (Top: Fast sheeting rate; Bottom: Slow sheeting rate).

.

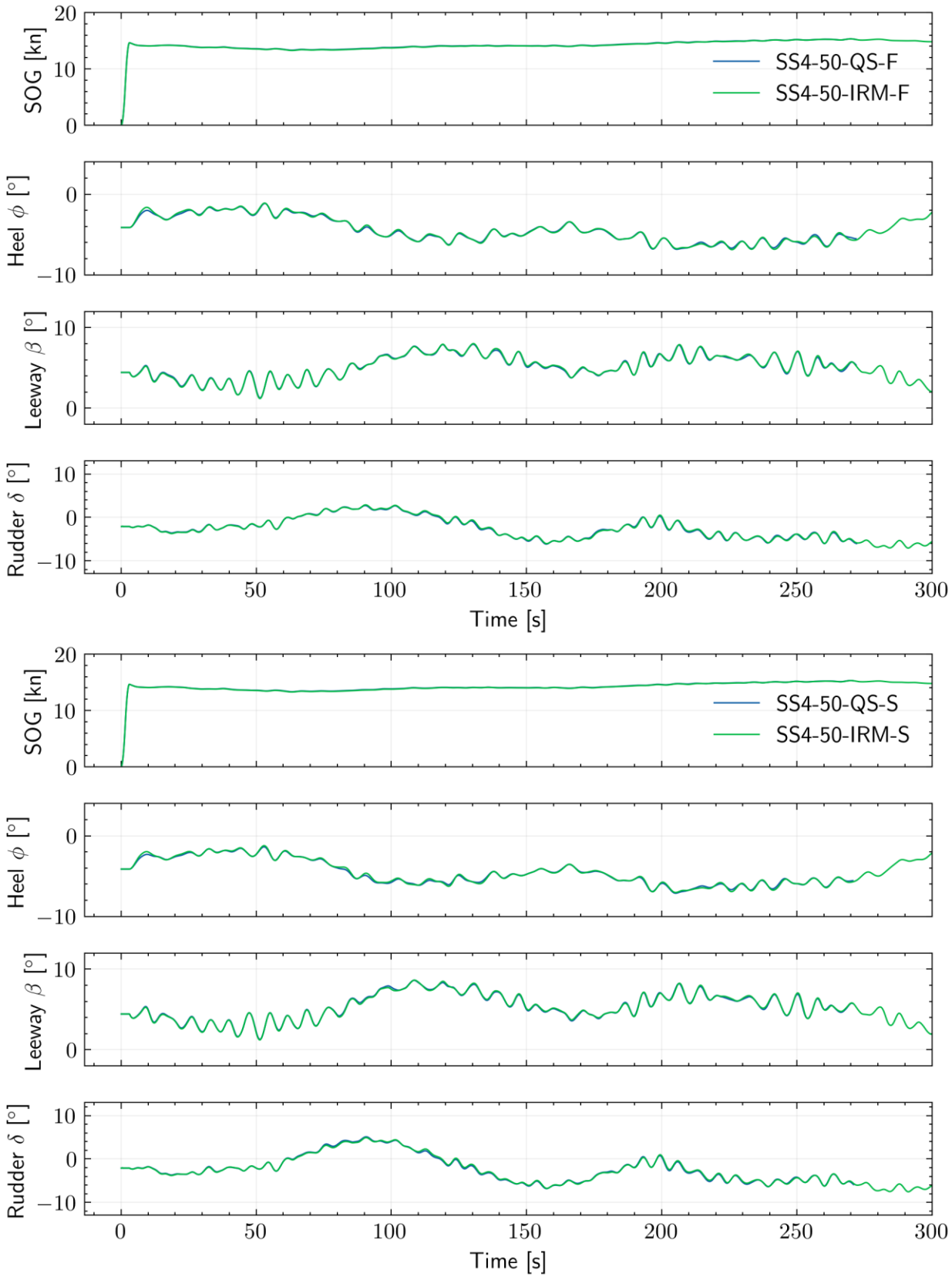

Figure 7 Time series of SOG, heel angle, leeway angle and rudder angle (Top: Fast sheeting rate; Bottom: Slow sheeting rate).

5. CONCLUSIONS

In this paper we have examined the influence of unsteady modelling of circulatory lift on the performance of a fully sailing car carrier in a moderate sea state (SS4, $H_S = 1.88$ m) and corresponding true wind speed of 10 m s^{-1}. Two different sheeting strategies were investigated, both being continuous adjustment of the sheet/boom angle for a target local angle of attack for each wing, but with two different maximum sheeting rates: 3.0° s^{-1} and 0.125° s^{-1}. The former is here considered a high rate, or fast sheeting, and the latter is on the other hand considered to be slow.

In terms of the global performance variables: speed over ground, leeway angle, heel/roll angle and rudder angle, the difference is negligible, and the sheeting rate does not seem influence the outcome to any significant degree in this case.

However, looking closely at the time history of roll angle, the roll angle is slightly more dampened in the case of the quasi-static method, which indeed is the expected behaviour. It is expected that in conditions with larger waves and with a wave period closer to the vessel's natural roll period, the effect of aerodynamic roll damping will turn out to be much more evident. Hence, the application of unsteady circulatory lift modelling may have greater bearing on seakeeping performance rather than energy efficiency performance.

6. FUTURE WORK

The next step will be to study the impact of modelling unsteady circulatory lift on cases with large amplitude roll motions, e.g., due to larger waves and longer wave period. Extreme aerodynamic loads on the wings due to strong gusts is also a potentially important topic to investigate.

7. ACKNOWLEDGEMENTS

The authors acknowledge the financial support from the European Commission and its agency CINEA, grant 101096673.

8. REFERENCES

Fossati, F., and S. Muggiasca, (2010) "Numerical Modelling of Sail Aerodynamic Behavior in Dynamic Conditions", In: Innovation in High Performance Sailing Yachts 2010, RINA, Lorient, France. doi:10.3940/rina.innovsail.2010.02.

Gerhardt, F.C., R.G.J. Flay, and P. Richards (2011). "Unsteady Aerodynamics of Two Interacting Yacht Sails in Two-Dimensional Potential Flow", Journal of Fluid Mechanics 668, 551–581. doi:10.1017/S0022112010004842.

Jones, R. T. (1938), "Operational treatment of the nonuniform-lift theory in airplane dynamics", Technical Note No. 667, NACA-TN-667, National Advisory Committee for Aeronautics, Langley Memorial Aeronautical Laboratory.

Kjellberg, M., F.C. Gerhardt, and S. Werner (2023). "Sailing Performance of Wind-Powered Cargo Vessel in Unsteady Conditions". In: Proceedings of the 6th International Conference on Innovation in High Performance Sailing Yachts and Wind-Assisted Ships, Lorient – France, May 29-31, 2023.

Persson, A., L. Larsson, and C. Finnsgård (2023). "A Time-Domain Model for Unsteady Upwind Sail Aerodynamics using the Indicial Response Method". Under review, pre-print published soon.

Roux, Y., A. Leroyer, M. Visonneau, J. Raymond, and F. Hauville (2008). “Strongly Coupled VPP and CFD RANSE Code for Sailing Yacht Performance Prediction”, In: Proceedings of the 3rd High Performance Yacht Design Conference, Auckland, New Zealand. pp. 215–226.

Spalart, P. R., and C. L. Rumsey (2007). “Effective Inflow Conditions for Turbulence Models in Aerodynamic Calculations”. AIAA Journal, Volume 45, Issue 10, pp. 2544-2553. DOI: 10.2514/1.29373.

Wagner, H. (1925). “Über die Entstehung des dynamischen Auftriebes von Tragflügeln”. Zeitschrift f. angew. Math. u. Mech. Bd. 5. 1925. S. 17 - 35.

Kármán, v., T., and M. A. Biot (1940). “Mathematical Methods in Engineering”. McGraw-Hill, New York.

Gerhardt, F. C., Flay R. G. J., and Richards, P. (2011) “Unsteady aerodynamics of two interacting yacht sails in two-dimensional potential flow,” *Journal of Fluid Mechanics*, vol. 668, pp. 551–581, doi: 10.1017/S0022112010004842.